Pediatric RESEARCH

www.nature.com/pr

CLINICAL RESEARCH ARTICLE

Ventricular remodeling in preterm infants: computational cardiac magnetic resonance atlasing shows significant early remodeling of the left ventricle

David J. Cox[1], Wenjia Bai[2], Anthony N. Price[1], A. David Edwards[1], Daniel Rueckert[2] and Alan M. Groves[3]

BACKGROUND: Premature birth is associated with ventricular remodeling, early heart failure, and altered left ventricular (LV) response to physiological stress.Using computational cardiac magnetic resonance (CMR) imaging, we aimed to quantify preterm ventricular remodeling in the neonatal period, and explore contributory clinical factors.

METHODS: Seventy-three CMR scans (34 preterm infants, 10 term controls) were performed to assess in-utero development and preterm ex-utero growth.End-diastolic computational atlases were created for both cardiac ventricles; *t* statistics, linear regression modeling, and principal component analysis (PCA) were used to describe the impact of prematurity and perinatal factors on ventricular volumetrics, ventricular geometry, myocardial mass, and wall thickness.

RESULTS: All preterm neonates demonstrated greater weight-indexed LV mass and higher weight-indexed end-diastolic volume at term-corrected age ($P < 0.05$ for all preterm gestations). Independent associations of increased term-corrected age LV myocardial wall thickness were (false discovery rate <0.05): degree of prematurity, antenatal glucocorticoid administration, and requirement for >48 h postnatal respiratory support.PCA of LV geometry showed statistical differences between all preterm infants at term-corrected age and term controls.

CONCLUSIONS: Computational CMR demonstrates that significant LV remodeling occurs soon after preterm delivery and is associated with definable clinical situations. This suggests that neonatal interventions could reduce long-term cardiac dysfunction.

Pediatric Research (2019) 85:807–815; https://doi.org/10.1038/s41390-018-0171-0

INTRODUCTION

Globally there are more than 15 million preterm births (prior to 37 weeks' gestation) per year. Advances in obstetric care and neonatal practice are improving survival rates and leading to an ever-increasing cohort of adults born prematurely.[1,2]

Premature birth is associated with hypertension, myocardial infarction, adult heart failure, and potentially early death from cardiac causes.[3–6] Recent studies have identified early impacts of prematurity on cardiac development and function including altered early myocardial development, heart failure in childhood, and altered left ventricular response to physiological stress.[7–9]

The phenotype of pathological cardiac development following premature birth was defined in young adults by the application of magnetic resonance imaging (MRI)-based cardiac atlases; this phenotype included altered human ventricular geometry, increased indexed myocardial mass, and associations with reduced biventricular function.[10–12] Whilst both cardiac ventricles are affected, studies in young adults suggest a greater functional impact on the ex-preterm right ventricle (RV) compared to the left ventricle (LV).[11] More recent echocardiographic studies have shown increased indexed LV and RV masses at 3 months in premature neonates, though early changes in LV geometry were thought to be transient.[7]

As many authors acknowledge, assumptions about ventricular geometry necessitate caution when interpreting echocardiographic-derived absolute mass measures and inferences on ventricular geometry, particularly for the RV.[7] However, optimized neonatal cardiac magnetic resonance (CMR) has demonstrated robust, validated in-vivo volumetric measurements of the preterm ventricles, and CMR atlasing is the proven gold-standard tool for generating robust cardiac geometries, though not previously tested for the neonatal population.[13–15]

This study adapted available neonatal CMR and adult computational atlasing techniques to confirm the hypothesis that preterm-associated ventricular remodeling originates in the neonatal period, demonstrate the phenotype of neonatal remodeling, and robustly explore associated clinical factors which could potentially offer future therapeutic targets.

METHODS

The study was approved by the North West London Research Ethics Committee (06/Q0406/137). All CMR scans were performed for research purposes only, written informed parental consent was obtained in all cases.

Study cohort

Preterm infants (born <37 weeks' gestation) and healthy term controls (born between 37–42 weeks gestational age (GA)) were recruited from the Neonatal Unit and postnatal wards of St

[1]Centre for the Developing Brain, King's College London, London, UK; [2]Department of Computing, Imperial College London, London, UK and [3]Icahn School of Medicine at Mount Sinai, New York, New York, USA
Correspondence: David J. Cox (david.cox@hee.nhs.uk)

Received: 11 April 2018 Revised: 1 August 2018 Accepted: 27 August 2018
Published online: 19 November 2018

Table 1. Patient characteristics of neonates contributing to the CMR computational atlases

Variable	Preterm subjects at baseline	Preterm subjects at term-corrected age	Term controls
Number of subjects	34	29	10
GA birth	$33^{+2}(24^{+2}-36^{+4})^{a}$	$31^{+5}(25^{+1}-36^{+4})^{a}$	$39^{+5}(37^{+1}-41^{+6})$
Corrected GA scan	$33^{+6}(25^{+1}-37^{+1})^{ab}$	$41^{+3}(39^{+5}-42^{+0})^{a}$	$40^{+1}(37+3-42^{+3})$
Day of scan	5.1 (3−7)[ab]	69.3 (33−136)[a]	3.5 (2−7)
Weight at scan (kg)	1.85 (0.71−2.94)[ab]	3.21 (2.28−4.44)	3.48 (2.84−3.92)
BSA at scan (m^2)	0.15 (0.08−0.21)[ab]	0.22 (0.18−0.27)	0.23 (0.20−0.25)
Gender (M:F ratio)	1.83:1	1.64:1	1:1
IUGR	7[a]	5[a]	0
Antenatal glucocorticoids	23[a]	25[a]	1
Diagnosed PDA	4[a]	5[a]	0
Respiratory support >48 h	10[a]	9[a]	0

Values given represent either absolute values or mean values with ranges in parentheses
[a]Denotes preterm cohort parameters with a difference of $P < 0.05$ from the "Term control" cohort
[b]Denotes parameters in the "Preterm subject at baseline" cohort with a difference of $P < 0.05$ from the "Preterm subjects at term-corrected age" cohort

Thomas' Hospital, London, UK, between 2012 and 2015. Study exclusion criteria were: contraindications to CMR scanning, congenital heart disease (transitional conditions such as patent foramen ovale (PFO) and patent ductus arteriosus (PDA) were not excluded), parents in whom obtaining consent was deemed non-ethical, and neonates deemed too sick to tolerate a CMR study by their consultant neonatologist.

Thirty-four preterm "baseline" CMR scans representing a surrogate of in-utero growth were performed within the first 7 days, and 29 "term-corrected age" scans were performed in preterm neonates at 37–42 weeks corrected gestational age (CGA) to allow description of ex-utero preterm cardiac development and facilitate direct comparison between preterm infants and ten healthy term-born controls (scanned within 7 days of birth). Further patient demographics are shown in Table 1.

The results of CMR scanning did not alter the neonates' clinical care; decisions on clinical management including investigation and treatment for PDA, use of inotropic and respiratory support, and nutritional/feeding regimen were governed entirely by the clinical team responsible for the neonates' care, who were blinded to the research findings.

Medical data collection

Data on antenatal history and neonatal care were collected from in-patient medical notes and electronic patient records. Structured data collection targeted factors postulated to affect cardiac remodeling including patient gender, intrauterine growth restriction (IUGR), antenatal glucocorticoid administration, postnatal inotrope use, PDA (defined in this study as clinical concern of PDA with confirmation of PDA on echocardiography; PDA treatment was at the discretion of individual clinicians and recorded separately), and mode and duration of respiratory support. All stored data, including MR data, were coded with subject- and study-specific identifiers to ensure anonymity and blinded analysis.

CMR imaging acquisition

All scans were performed using a "feed and wrap" free-breathing technique without sedation or anesthesia, as described previously by Merchant et al.[16]

CMR data were acquired on a Philips 3.0-Tesla MR Achieva scanner (Best, Netherlands) using a specialized 8-channel pediatric body receive coil for neonates >2 kg, and an 8-channel small extremity receive coil for neonates <2 kg. Neonatal CMR scanning and parameter optimization has been previously described by Price et al.[15] Steady-state free-precession (SSFP) cine sequences were acquired to localize cardiac anatomy, before acquisition of an optimized retrospectively-VCG-gated 2D SSFP 10-slice short axis cine stack. SSFP image acquisition parameters were: acquired in-plane resolution 1 × 1 mm; 20 retrospectively gated phases per cardiac cycle, average temporal resolution 22.2 ms (range 17.6–33.3 ms); slice thickness 4 mm; repetition time 3.8 ms; echo time 1.9 ms; flip angle 35°; four signal averages. Varied negative inter-slice gap, enabled interpolation of slice thickness to below 4 mm whilst ensuring full coverage from apex to base of the both ventricles in all individuals. The post-processing steps further interpolated the slice thickness to achieve a reconstructed isotropic voxel resolution. No CMR-acceleration methods or respiratory gating techniques were used; acquisition time ranged between 4 and 6 min. Anonymized CMR data were stored on a protected digital archive for subsequent analysis.

CMR data post-processing

All post-processing was performed on end-diastolic (ED) CMR frames. Short-axis and 4-chamber DICOM files were visualized and segmented using Segment v1.8 R1172 software (segment.heiberg.se)[17] to quantify ventricular cavity volume, ensuring correct ED frame selection.

Ventricular computational atlas creation

Image segmentation. The ED datasets were converted to NIfTI (Neuroimaging Informatics Technology Initiative) format. Segmentation was performed by a single researcher, with 9 months prior training, using ITK-SNAP dedicated image segmentation software (www.itksnap.org) which allows for semi-automatic segmentation using active contour methods and manual delineation.[18] While various software programs are available for cardiac segmentation, ITK-SNAP was chosen due to previous researcher experience of robust performance in segmenting neonatal CMR datasets and the availability of a seed-based "Snake" tool which allowed for region-growing, level-set segmentation. Ventricular myocardium and blood pools were labeled through manual tracing of the endo- and epicardial borders for each slice. The LV outflow tract was included in the ventricular blood pool volume when representing <50% of the LV blood volume on the slice, and the papillary muscles were excluded from the myocardial segmentation and included in the LVEDV to facilitate more robust subsequent image registration. RV segmentation followed similar principles and

techniques to that of the LV, however segmentation of the RV included regions of the interventricular septum considered to be RV in developmental origin due to the smooth geometric continuity with the RV free wall mass. Image segmentation provided quantification of ventricular myocardial mass from volume ((ED epicardial–endocardial volume) × 1.05) and EDV (endocardial volume) for both RV and LV for each subject; 1.05 g/ml representing the predicted density of myocardial tissue.

Image registration. Image registration techniques were performed using Image Registration Toolkit software (IRTK, www.doc.ic.ac.uk/~dr/software/).[19–21] The segmented datasets were manually landmarked using LV and RV landmarks including the myocardial apex, and septal mid-point, RV insertion points and center of the blood pool at mid-ventricular and basal levels. Landmarks were chosen based on apparent reliability and repeatability of assessment in the context of a known paucity of true anatomical landmarks identifiable on cine MR scanning. The registration and atlasing technique used had previously been optimized and validated for neonatal CMR data and followed the principles described by Frangi et al.[22] First, a point-based rigid registration of the anatomical landmarks is used to align the segmentations to a common coordinate system. A voxel-based multi-resolution, free-form, non-rigid registration algorithm was used to warp individual segmentations to a pre-assigned template, the target segmentation. The chosen template segmentation was the dataset with highest segmentation repeatability and robustness of landmarking. The non-rigid registration algorithm embedded labeled segmentations into a multi-nodal volumetric mesh through modeling the spatial deformation between images as an interpolated field governed by a set of B-spline basis functions. The deformation was progressively refined through multiple resolution stages by increasing the density of the B-spline modes.[16]

Unbiased templates for each ventricle were created through a 2-step iteration; initial registration to an assigned, biased, target segmentation to warp all segmentations to a common coordinate space, with subsequent averaging forming unbiased LV and RV templates. Repetition of the registration process registered all segmentations to the unbiased templates, producing deformation field files detailing the size and shape difference of all patient segmentations relative to the unbiased template. Individual warped segmentations, produced through application of the deformation field files to the unbiased templates, were resampled using shape-based interpolation and the application of a marching cubes algorithm created individual surface meshes facilitating visualization and statistical analysis.

Neonatal ventricular atlas construction. Patients were grouped into cohorts by GA at birth. Concatenation of deformation fields within a cohort created atlases representative of that population. Five preterm cohorts were created that spanned the viable preterm GA range: neonates born <26 weeks, 26–29 weeks, 29–32 weeks, 32–35 weeks, and 35–37 weeks. Each cohort had two sets of atlases created, at baseline and at term-corrected age. An atlas was also produced for the healthy term control cohort. Dice similarity coefficients (DSC) were used to analyze how robustly cohort atlases represented all individual constitutive patients.[23] Myocardial and ventricular blood pool surface meshes were composed of 27,797 and 14,099 mesh points, respectively, for the LV, and 28,986 and 14,798 mesh points for the RV. Each mesh point identified spatial location, with the myocardial surface mesh points providing additional data on local wall thickness.

Statistical analysis

Statistical analysis was performed using SPSS version 22 and MATLAB R2015a (Mathworks, Natick, MA). Comparison of continuous variables within patient groups was conducted with a 2-sided, independent samples Student's *t*-test where data were normally distributed; categorical variables were compared with a χ^2 test.

Myocardial mass and end-diastolic volume (EDV) data were indexed for patient weight at the time of scan.

Standardization of the number of nodes and alignment of myocardial meshes allowed calculation of mean wall thickness at every nodal point. Generated *P*-values were corrected for multiple comparisons by adjusting for false discovery rate (FDR). Assessment of perinatal factors associated with altered wall thickness was performed by regression analysis using the principles of generalized linear modeling with an ANCOVA.[24] Principal component analysis (PCA) was performed to identify the key modes of shape variation in preterm hearts at term-corrected age—the parametric space was reduced from >14,000 modes of variation to the principal 10 which accounted for approximately 95% of the shape variation seen for each ventricle. Throughout the reported results, values of $P < 0.05$ (after correction for multiple comparisons) were considered significant.

RESULTS

Study population characteristics

Baseline demographics, clinical parameters and scan timings for the preterm, preterm at term, and term control cohorts are shown in Table 1.

Table 2. Weight-indexed ventricular mass, end-diastolic volume, and growth values for the different preterm cohorts

Cohort	LV mass (g/kg)	LV end-diastolic volume (ml/kg)	Growth vs. Term control cohort (%)		RV mass (g/kg)	RV end-diastolic volume (ml/kg)	Growth vs. Term control cohort (%)	
	Baseline (< 7 d)		LVm	LVEDV	Baseline (< 7 d)		RVm	RVEDV
< 29 weeks	1.41	2.81	−29.8	−17.4	1.63	2.36	−41.1	18.2
29–32 weeks	1.16	2.72	−14.7	−14.7	1.01	3.07	−5.0	−9.1
32–35 weeks	1.13	2.86	−12.4	−18.9	0.99	3.10	−3.0	−10.0
35–37 weeks	1.09	2.78	−9.2	−16.5	1.00	3.04	−4.0	−8.2
	Term corrected		LVm	LVEDV	Term corrected		RVm	RVEDV
< 29 weeks	1.64	3.49	16.3	24.2	1.18	3.27	−27.6	38.6
29–32 weeks	1.52	3.59	31.0	32.0	1.11	3.41	9.9	11.1
32–35 weeks	1.35	3.36	19.5	17.5	1.04	3.12	5.1	0.6
35–37 weeks	1.25	3.17	14.7	14.0	0.92	2.94	8.0	−3.3
Term controls	**0.99**	**2.32**	–	**0.96**	**2.79**	–	–	

Mean values for weight-indexed measurements

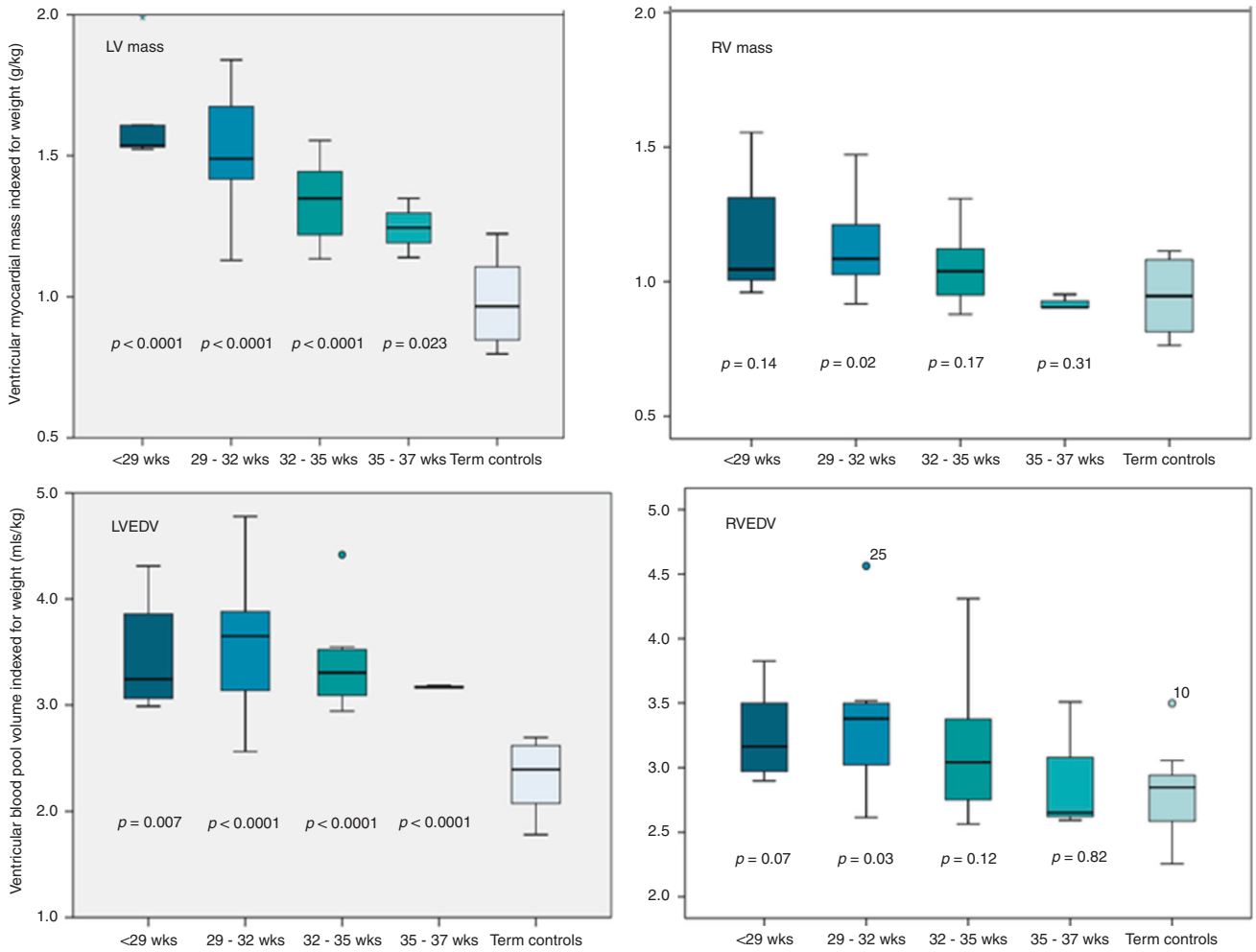

Fig. 1 Graphs showing ventricular volumetrics for preterm cohorts indexed for weight; *P*-values compare preterm cohorts with term controls. Boxplots represent median and interquartile ranges for each cohort

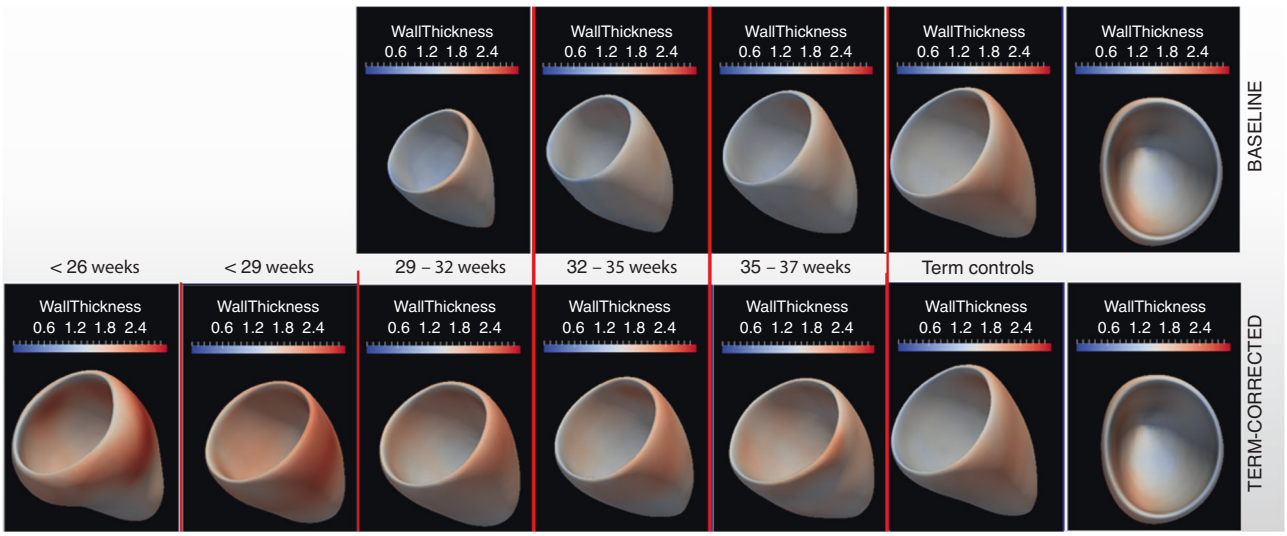

Fig. 2 Graphic showing left ventricular myocardial atlases for the different gestational age cohorts at baseline and at term-corrected age. Point myocardial wall thickness in millimeters demonstrated by color

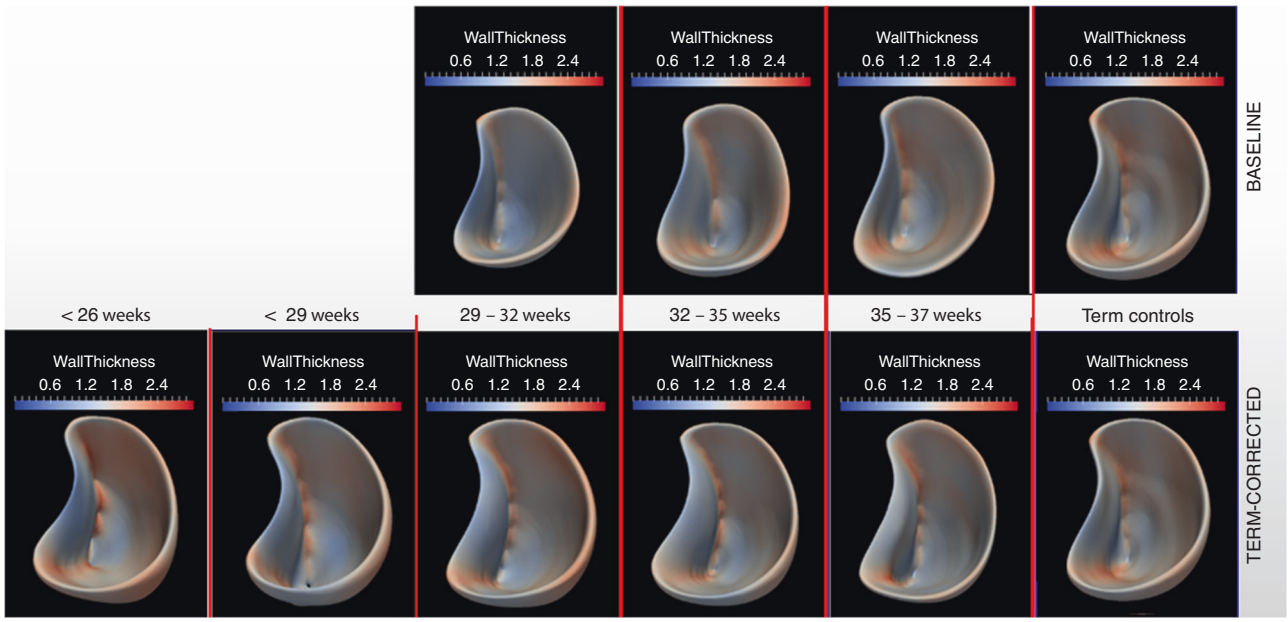

Fig. 3 Graphic showing right ventricular myocardial atlases for the different gestational age cohorts at baseline and at term-corrected age. Point myocardial wall thickness in millimeters demonstrated by color

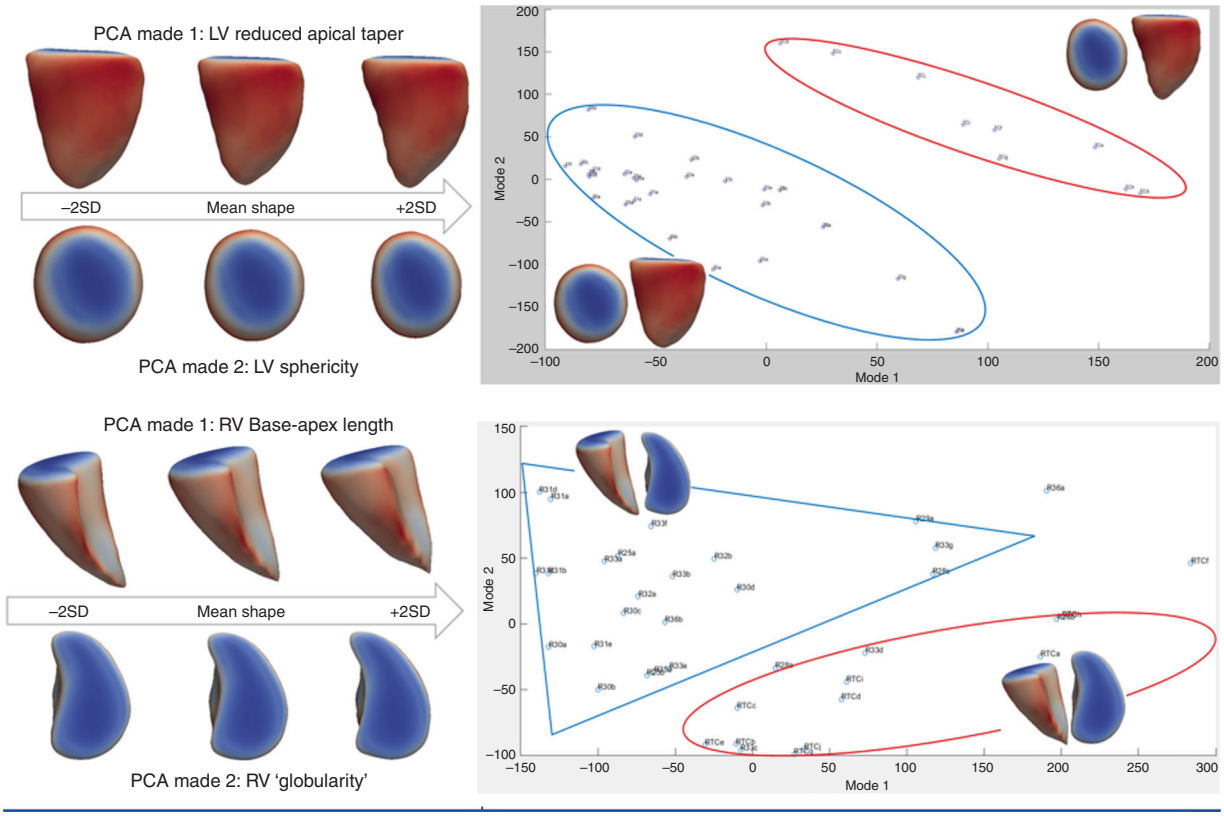

Fig. 4 Principal component analysis (PCA) defined main two modes of shape variation in neonatal left and right ventricles at term-corrected age. Red ellipse encompasses all term controls for the left ventricle (top graph), and most term controls for the right ventricle (lower graph); blue shapes encompass all preterm-born left ventricles at term-corrected age (top graph), and the majority of preterm-born right ventricular geometries (lower graph)

Elevated weight-corrected ventricular mass and EDV in preterm cohorts

Postnatal baseline assessment (scans performed within 7 days of life) in all cohorts born >29 weeks GA demonstrated higher weight-indexed values for RVEDV than for LVEDV, but reduced weight-indexed RV mass (RVm) compared with LV mass (LVm) for equivalent GA (Table 2).

All preterm cohorts scanned at term-corrected age demonstrated greater mean indexed values ($P < 0.05$) for LVm and LVEDV than healthy term controls; calculated ex-utero weight-indexed

growth percentages showed increases between 14.0 and 32.0% for both in LVm and LVEDV contrasting with reduction in weight-indexed in-utero percentage values of similar magnitude (Table 2 and Fig. 1). Infants born at <29 weeks demonstrated 64% greater weight-indexed LVm at term-corrected age than the term control cohort (1.64 ± 0.04 vs. 0.99 ± 0.17 g/kg, $P < 0.0001$).

Whilst a trend toward greater mean indexed RVm and RVEDV was noted for preterm-born infants at term-corrected age compared with the term-born control cohort, the only preterm cohort in which a statistically significant difference was noted was the cohort born between 29 and 32 weeks GA (Table 2, Fig. 1).

Values for LV and RV myocardial mass and EDV indexed for body surface area (BSA) correlated closely with the respective weight-indexed values for preterm cohorts scanned at term-corrected age. However, there was a significant discrepancy between the weight and BSA indexed values for preterm cohorts at baseline; this is likely due to the challenges in obtaining accurate BSA values for sick preterm infants. (Supplemental Tables S1–S2 (online)). Weight-indexed values were used to draw conclusions on cardiac development due to the improved accuracy of assessment in the neonatal population.

Computational neonatal ventricular atlas creation and analysis
Nine cohort atlases of similarly matched GA were created for each ventricle, displaying shape and computed myocardial wall thickness values (Figs. 2 and 3). Dice similarity metrics demonstrated the generated atlas for each cohort to be unbiased toward individual constituent scans; comparison of atlases with individual scans from other cohorts demonstrated the specificity of an atlas to their GA cohort (Supplemental Tables S3–S6 (online)).

LV shape analysis. Baseline scans were conducted within the first 7 days in an attempt to limit the impact of early postnatal pathophysiological remodeling. Significant changes in postnatal ventricular volumes may occur over the first few days. However, visual analysis of the consistency of LV geometry and LV wall thickness observed in the postnatal baseline atlases, despite images having been taken at a range of 3–7 postnatal days, suggests relatively uniform third trimester in-utero development and early postnatal adaptation. This correlates with the quantified increases in absolute LVm and LVEDV (Table 2 and Fig. 2).

PCA performed on all LV models created from term-age equivalent scans showed two leading modes accounting for 57% of the population's LV geometric shape variation (mode 1 = 35%, mode 2 = 22%). Mode 1 altered LV tapering toward the apex of the ventricle, mode 2 affected LV cavity diameter between the septum and lateral free wall (Fig. 4). A clear distinction in shape was seen between all the preterm infants scanned at term-corrected age and the healthy term controls; preterm hearts demonstrating a more globular LV shape with more spherical blood pool (Fig. 4, mode 1 $P < 0.0001$; mode 2 $P = 0.003$).

RV shape analysis. Visual analysis and growth percentage comparison of RV cohort atlases constructed from postnatal

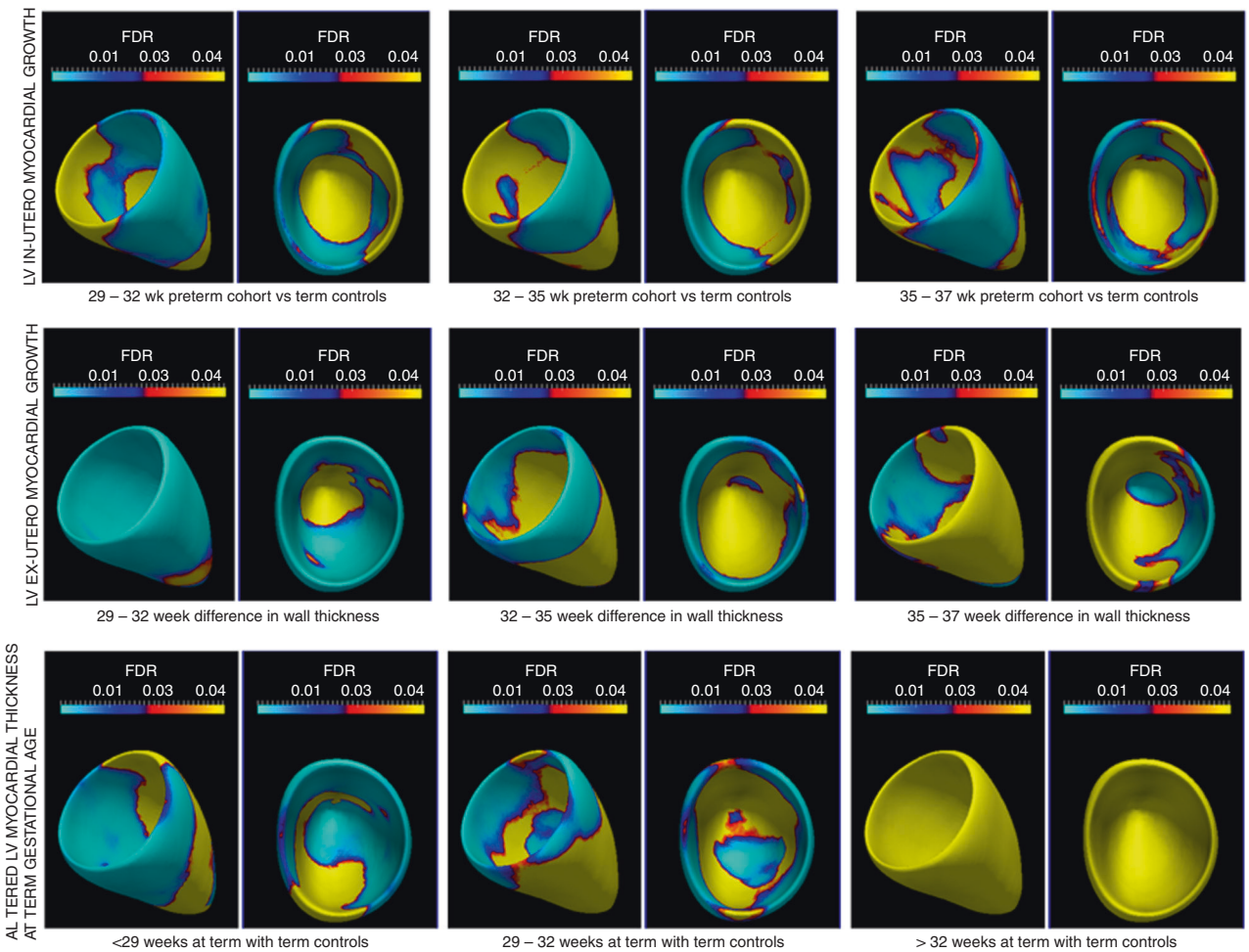

Fig. 5 Graphic contrasting in-utero and ex-utero left ventricular myocardial wall thickness change up to term-corrected age; non-significant change (FDR > 0.05) depicted by yellow color, all other colors indicate significant differences (FDR < 0.05) between cohorts at term-corrected age

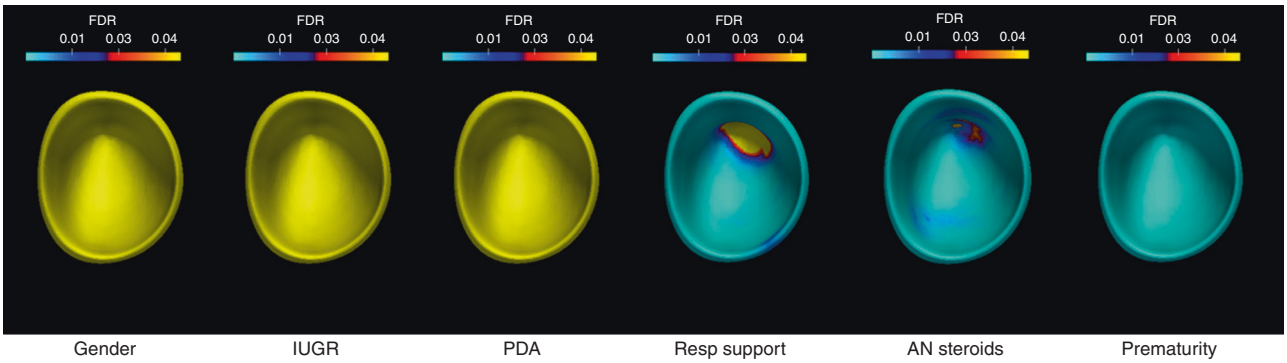

Fig. 6 Fetal and neonatal factors associated with alterations in left ventricular myocardial wall thickness in preterms at term-corrected age compared to term controls; areas of increased myocardial wall thickness meeting statistical significance at FDR < 0.05 shown by non-yellow colors on ventricular models

baseline CMR scans again suggested consistent in-utero ventricular growth and early postnatal volumetric adaptation, with RV shape preservation from 29 weeks' gestation (Table 2 and Fig. 3). The preterm RVs scanned at term-corrected age displayed very similar size and shape characteristics to term controls (Fig. 3). PCA performed on all RV models created from term-equivalent scans again showed two modes of variation accounting for approximately 60% of the population's RV geometric variation (mode 1 = 47.5%, mode 2 = 13%). Mode 1 altered RV base–apex length, mode 2 affected the RV blood pool shape, particularly septal wall curvature—termed "globularity" for the purpose of graphical demonstration (Fig. 4). No statistically significant differences in RV shape were observed between preterm infants scanned at term-corrected age and the healthy term controls; however, graphical representation demonstrated clustering of preterm RV geometry toward greater ventricular base–apex length and more pronounced septal curvature (Fig. 4).

LV regional wall thickness analysis. Assessment of different cohorts with paired *t*-tests generated FDR-corrected *P*-value maps showing myocardial regions with statistically significant differences in wall thickness. Surrogates of in-utero growth (comparison of preterm ventricles at baseline vs. healthy term-born controls) show consistent significant increases in weight-indexed wall thickness in the LV septal region throughout the third trimester (Fig. 5). Myocardial wall thickness values in other regions increased at a lower rate, not reaching statistical significance. Ex-utero myocardial development through the third trimester (comparison of the preterm ventricles at baseline and term-corrected age) displayed contrasting and more diffuse patterns of statistically significant LV wall thickness growth (Fig. 5).

Postnatal myocardial remodeling was assessed by comparing wall thickness in preterm cohorts at term-corrected age with healthy term controls. Neonates born <29 weeks had large areas of statistically significant point-registered LV myocardial thickening, encompassing greater than 50% of the LV and including the septal and free ventricular walls. As preterm GA at birth increased, the total area of altered LV myocardial thickness decreased (Fig. 5).

RV regional wall thickness analysis. Analysis of in-utero RV growth, ex-utero RV myocardial development, and postnatal RV remodeling did not demonstrate any regions of myocardium with statistically significant wall thickness change after correction for FDR.

Perinatal factors affecting wall thickness remodeling. Generalized linear modeling on all term-age ventricular models, with statistical parametric mapping of the ventricles, allowed independent assessment of multiple clinical covariates.[18] The results were processed to show regions of statistically significant increases in myocardial wall thickness affected by each covariate and demonstrated on standardized myocardial meshes. All quoted *P*-values are post FDR correction.

The degree of prematurity was strongly associated with changes in wall thickness over the whole LV ($P < 1 \times 10^{-5}$ for all nodes). Clear independent associations were also observed for requirement for respiratory support >48 h and the administration of antenatal glucocorticoids—the majority of the LV was affected ($P < 0.05$) with sparing only at the ventricular apex. Very little association was seen between LV wall thickness and PDA, IUGR, or gender (Fig. 6).

RV analysis revealed no perinatal factors associated with wall thickness change after correction for FDR.

DISCUSSION

Computational atlasing of neonatal cardiac MRI data demonstrates that premature birth causes definable changes to LV mass, wall thickness, EDV and geometry in the neonatal period, which were quantifiably greater for birth at earlier gestation (Figs. 1 and 6).

Impact of prematurity on LVm, wall thickness, and EDV

The extent of the observed change in preterm neonatal LVm broadly correlates with recent echocardiographic data in the first 3 months of life but is greater than the approximate 20% increase in biventricular mass quantified by computational cardiac CMR atlasing studies in young adults.[7,10] Our results show premature infants born at <29 weeks demonstrate a 64% greater indexed-LVm at term-corrected age than healthy term-born controls. Whilst previous research has indicated that cardiac growth tracks from early postnatal life into childhood, and from childhood to adult life, we believe future longitudinal studies are required to demonstrate if, and when, the large increase in indexed LVm regresses to that observed in studies at young adulthood.[25,26] Increased LVm is an independent risk factor for cardiovascular morbidity and mortality; if the increases in observed LVm do persist into adulthood, this degree of increased LVm would likely lead to significantly elevated risk of clinical cardiovascular events later in life.[6,27]

Our preterm cohort demonstrated significant increases in LVEDV compared to term-born controls, whereas young adults born prematurely display decreased LV chamber volumes. Increased neonatal LVEDV might be expected due to physiological adaptation to increased postnatal pulmonary venous return, particularly in the presence of a PDA.

Increased LV wall thickness was independently associated with degree of prematurity, antenatal glucocorticoid exposure, and respiratory support requirement for >48 h. Association between steroid administration and cardiac hypertrophy in the newborn

period is well-described, though in most cases the effect is felt to be transient.[28–30] However, exposure to antenatal glucocorticoids impacts key regulators of cardiac function and maturation of the developing myocardium such that longer term programming may be effected.[31]

Respiratory support may be only casually associated with LV remodeling, since infants with circulatory compromise generally require respiratory support. However, respiratory support also impacts lung volume, intrathoracic pressure, venous return, and coronary artery flow, and the mechanics of myocardial contraction; all of which could contribute to remodeling.[32]

Impact of prematurity on LV shape

PCA showed preterm neonates to have more globular hearts with more spherical shape. Mann et al. commented that increased LV sphericity is one of the first observations of pathophysiological significance in LV remodeling.[33] The mechanisms leading to the development of this spherical shape in preterm hearts are likely to be similar to those seen in adult cardiomyopathies.[34] The change from ellipse to more spherical LV shape increases meridional wall stress and so creates a further energetic burden for the immature myocardium.[33] The long-term prognostic significance of neonatal LV shape change is unclear, though in adult patients greater LV sphericity is associated with heart failure, reduced exercise tolerance, and an increased incidence of mitral regurgitation.[35,36] Any increased neonatal LV sphericity that compromised future valvular integrity would lead to greater LV preload and a potential cycle of adverse LV remodeling.

Pathophysiology underlying neonatal LV remodeling

Overall, very little is definitively known about pathophysiology of LV remodeling in human preterm cohorts. It has been hypothesized that remodeling occurs secondary to changes in ventricular workload resulting from differences in preload, intracardiac flow pattern, and afterload. Shunting of blood through a PDA is a common cause for increased preload in preterm infants and has previously been associated with increased LVm in the neonatal period.[13] However, our study did not detect a significant association between PDA and remodeling of either ventricle; we did not systematically assess preterm patterns of disrupted intracardiac flow which result in reduced kinetic energy maintenance, and may necessitate greater preload to maintain sufficient cardiac function.[37] Our findings may have been affected by the low number of neonates with PDA in the study and association of PDA with co-variates of earlier GA, receipt of antenatal glucocorticoids, and need for prolonged respiratory support, making identification as an independent risk modifier more challenging. Study of a larger cohort is required before drawing definitive conclusions on the effect of PDA on ventricular remodeling.

The functional and histological immaturity of the preterm myocardium leaves it vulnerable to increases in afterload in the neonatal period, including cord-clamping and medical therapies such as inotropes and vasopressors.[38,39] The consequence of a sustained high afterload on immature myocardium may be early adaptive myocardial hypertrophy, with the later corollary being persistence of hypertrophic remodeling.

Preterm lamb models show five- to sevenfold increases in neonatal interstitial collagen deposition, and evidence of myocardial fibrosis.[40] Myocardial growth and compliance is dependent upon optimal cellular and extracellular matrix composition, and similar findings in humans would alter the mechanical scaffold of the heart and likely restrict normal LV cavity growth.

Hyperoxia may be a further trigger for preterm cardiac remodeling. In small animal models, transient exposure to hyperoxia produces long-term cardiac remodeling and vulnerability to early cardiac failure.[41] These changes appear to be mediated by alterations in renin–angiotensin activity. Preterm infants are exposed to relative hyperoxia (50–70 mmHg) compared to the fetal environment (30–40 mmHg) and hyperoxia may be compounded by supplemental oxygen therapy for respiratory disease. Preterm neonates exhibit prolonged alterations in renin–angiotensin activity with higher levels of angiotensin II in infants with respiratory disease.[42]

Remodeling of the preterm RV

Surrogates for in-utero ventricular blood pool volumetrics from >29 weeks GA demonstrated consistently greater indexed-RVEDV values when compared to the LV, in keeping with perceived fetal right ventricular dominance.[43] Changes in RV growth in the neonatal period were significantly reduced compared with the LV, with non-significant increases in indexed RVm and RVEDV for most GA cohorts at term-corrected age. This again contrasts with Lewandowski et al. who showed a greater increase in RVm than LVm in young adults.[11] However, the dominant fetal RV shows a relative regression in healthy term newborns as pulmonary vascular resistance falls and the RV no longer contributes to systemic perfusion. During this process, the RV loses around 40% of its bodyweight-indexed mass. We compared our preterm infants to a cohort of term newborns yet to undergo the physiologic reduction in RVm. Therefore, a weight-indexed RVm increase of 22% in infants born <29 weeks may actually demonstrate a significant failure of RVm regression rather than an absence of significant growth increase. Our study suggests increased preterm-related indexed RVEDV in the neonatal period, compared to the decrease seen in young adults. Again whether the change we have observed in the neonatal period will persist through childhood is currently unknown.

Study limitations

This study provides only single-center insight into neonatal cardiac remodeling and though computational atlasing facilitates statistically powerful information from comparatively few scans, the number of studied infants was relatively small. Different patient populations and neonatal care practices may produce different patterns of remodeling.

A notable limitation was that comparative measures of normal development were only taken from a term control group scanned within 7 days of birth. As neonates undergo significant circulatory transition and cardiac adaptation after birth, it would have been useful to assess and document normal development of healthy term neonatal ventricles with repeat scanning and computational atlasing at 4–6 weeks of postnatal age. Whilst there is literature suggesting what these outcomes may be, there would be value in using the same assessment technique in an older term cohort to complete the understanding of what constitutes normal development as opposed to pathological early remodeling.

Our technique for left ventricular segmentation differs from that of the Society of Cardiovascular Magentic Resonance (SCMR) consensus status due to difficulties visualizing the aortic valve and robustly planning short axis stacks along the basal plane of the atrioventricular valve.[44] However, the repeatability metrics for the technique allied to our close correlation of DSC values, for LV cohorts particularly, lends support to the use of our technique for these datasets and the applicability of remodeling results for all analyzed preterm infants.

CONCLUSIONS

Cardiac remodeling associated with premature birth occurs in the neonatal period and leads to alterations in left ventricular mass, volume, and shape. The degree of hypertrophic and geometric remodeling in the most prematurely born infants demonstrated in this study is significant and, if sustained, may explain the increased cardiovascular morbidity and mortality observed in young adults.

Further research is required to understand the pathophysiology, but with increasing evidence suggesting early ventricular remodeling occurs, and preterm infants suffer long-term health impacts, the neonatal period may provide a potential diagnostic and future therapeutic window.

ACKNOWLEDGEMENTS

The Image Registration Toolkit was used under Academic License from Ixico Ltd. This study was supported by the Centre for the Developing Brain, King's College London & Department of Computing, Imperial College London. Funding for the study was received from the Medical Research Council & SPARKS Children's Medical Research charity (in the form of a Clinical Research Fellowship grant for Dr. David Cox, 2012–2015).

AUTHOR CONTRIBUTIONS

Substantial contributions to conception and design, acquisition of data, or analysis and interpretation of data—D.J.C., W.B., A.N.P., D.R., A.D.E. and A.M.G. Drafting the article or revising it critically for important intellectual content—DJ.C., W.B., A.N.P., D.R., A.D.E. and A.M.G. Final approval of the version to be published—D.J.C., A.D.E. and A.M.G.

ADDITIONAL INFORMATION

The online version of this article (https://doi.org/10.1038/s41390-018-0171-0) contains supplementary material, which is available to authorized users.

Competing interests: The authors declare no competing interests.

Publisher's note: Springer Nature remains neutral with regard to jurisdictional claims in published maps and institutional affiliations.

REFERENCES

1. World Health Organization, Media Centre. *Preterm Birth*. Fact sheet No. 36; Updated November 2014.
2. Beck, S. et al. The worldwide incidence of preterm birth: a systematic review of mortality and morbidity. *Bull. World Health Organ.* **88**, 31–38 (2010).
3. Barker, D. J., Eriksson, J. G., Forsén, T. & Osmond, C. Fetal origins of adult disease: strength of effects and biological basis. *Int. J. Epidemiol.* **31**, 1235–1239 (2002).
4. Centra, J. C., Roberts, G., Opie, G., Chong, J. & Doyle, L. W. Masked hypertension in extremely preterm adolescents. *J. Paediatr. Child Health* **51**, 1060–1065 (2015).
5. Bassareo, P. P. & Fanos, V. Editorial: cardiovascular drug therapy in paediatric age: from metabolomics to clinical practice. *Curr. Med. Chem.* **21**, 3107 (2014).
6. Crump, C., Sundquist, K., Sundquist, J. & Winkleby, M. A. Gestational age at birth and mortality in young adulthood. *J. Am. Med. Assoc.* **306**, 1233–1240 (2011).
7. Aye, C. Y. L. et al. Disproportionate cardiac hypertrophy during early postnatal development in infants born preterm. *Pediatr. Res.* **82**, 36–46 (2017).
8. Carr, H., Cnattingius, S., Granath, F., Ludvigsson, J. F. & Edstedt Bonamy, A.-K. Preterm Birth and risk of heart failure up to early adulthood. *J. Am. Coll. Cardiol.* **69**, 2634–2642 (2017).
9. Huckstep, O. J. et al. Physiological stress elicits impaired left ventricular function in preterm-born adults. *J. Am. Coll. Cardiol.* **71**, 1347–1356 (2018).
10. Lewandowski, A. J. et al. Preterm heart in adult life: cardiovascular magnetic resonance reveals distinct differences in left ventricular mass, geometry, and function. *Circulation* **127**, 197–206 (2013).
11. Lewandowski, A. J. et al. Right ventricular systolic dysfunction in young adults born preterm. *Circulation* **128**, 713–720 (2013).
12. Lewandowski, A. J. et al. Breast milk consumption in preterm neonates and cardiac shape in adulthood. *Pediatrics* **138**, e20160050 (2016).
13. Broadhouse, K. M. et al. Cardiovascular magnetic resonance of cardiac function and myocardial mass in preterm infants: a preliminary study of the impact of patent ductus arteriosus. *J. Cardiovasc. Magn. Reson.* **16**, 54 (2014).
14. Groves, A. M. et al. Functional cardiac MRI in preterm and term newborns. *Arch. Dis. Child. Fetal Neonatal Ed.* **96**, F86–F91 (2011).
15. Price, A. N. et al. Neonatal cardiac MRI using prolonged balanced SSFP imaging at 3T with active frequency stabilization. *Magn. Reson. Med.* **70**, 776–784 (2013).
16. Merchant, N. et al. A patient care system for early 3.0 Tesla magnetic resonance imaging of very low birth weight infants. *Early Hum. Dev.* **85**, 779–783 (2009).
17. Heiberg, E. et al. Design and validation of segment – a freely available software for cardiovascular image analysis. *BMC Med. Imaging* **10**, 1 (2010).
18. Yushkevich, P. A. et al. User-guided 3D active contour segmentation of anatomical structures: significantly improved efficiency and reliability. *Neuroimage* **31**, 1116–1128 (2006).
19. Rueckert, D. et al. Non-rigid registration using free-form deformations: application to breast MR images. *IEEE Trans. Med. Imaging* **18**, 712–721 (1999).
20. Schnabel J.A. et al. A Generic Framework for Non-rigid Registration Based on Non-uniform Multilevel Free-Form Deformations. In: Niessen W.J., Viergever M.A. (eds.) Medical Image Computing and Computer-Assisted Intervention – MICCAI 2001. MICCAI 2001. Lecture Notes in Computer Science, Vol **2208**, 573–581. Springer, Berlin, Heidelberg (2001).
21. Studholme, C., Hill, D. L. G. & Hawkes, D. J. An overlap invariant entropy measure of 3D medical image alignment. *Pattern Recognit.* **32**, 71–86 (1999).
22. Frangi, A. F., Rueckert, D., Schnabel, J. A. & Niessen, W. J. Automatic construction of multi-object three dimensional statistical shape models: application to cardiac modeling. *IEEE Trans. Med. Imaging* **21**, 1151–1166 (2002).
23. Crum, W. R., Camara, O. & Hill, D. L. G. Generalized overlap measures for evaluation and validation in medical image analysis. *IEEE Trans. Med. Imaging* **25**, 1451–1461 (2006).
24. Kiebel, S.J. & Holmes, A.P. (2003) The General Linear Model in Human Brain Function. In: Frackowiak, R.S.J. et al (eds) Human Brain Function, 2nd edn. Academic Press, P 725-760. https://doi.org/10.1016/B978-0-12-264841-0.X5000-8
25. Janz, K. F., Dawson, J. D. & Mahoney, L. T. Predicting heart growth during puberty: the Muscatine Study. *Pediatrics* **105**, 63 (2000).
26. Geelhoed, J. J. M. et al. Cardiac structures track during the first 2 years of life and are associated with fetal growth and haemodynamics: the Generation R Study. *Am. Heart J.* **158**, 71–77 (2009).
27. Loral, B. H. & Carabello, B. A. Left ventricular hypertrophy: pathogenesis, detection, and prognosis. *Circulation* **102**, 470–479 (2000).
28. de Vries, W. B., van der Leij, F. R., Bakker, J. M., Kamphuis, P. J., van Oosterhout, M. F., Schipper, M. E., Smid, G. B., Bartelds, B. & van Bel, F. Alterations in adult rat heart after neonatal dexamethasone therapy. *Pediatr. Res.* **52**, 900–906 (2002).
29. Paech, C., Wolf, N., Thome, U. H. & Knüpfer, M. Hypertrophic intraventricular flow obstruction after very-low-dose dexamethasone (Minidex) in preterm infants: case presentation and review of the literature. *J. Perinatol.* **34**, 244–246 (2014).
30. Vimala, J., Prabhu, A., Pavithran, S. & Kumar, R. N. Hydrocortisone induced hypertrophic cardiomyopathy. *Int. J. Cardiol.* **150**, e94–e95 (2011).
31. Eiby, Y. A. et al. Endogenous angiotensins and catecholamines do not reduce skin blood flow or prevent hypotension in preterm piglets. *Physiol. Rep.* **23**, e12245 (2014). pii.
32. Haruki, N. et al. Comparison of acute and chronic impact of adaptive servo-ventilation on left chamber geometry and function in patients with chronic heart failure. *Eur. J. Heart Fail.* **13**, 1140–1146 (2011).
33. Mann, D. L., Bogaev, R. & Buckberg, G. D. Cardiac remodeling and myocardial recovery: lost in translation? *Eur. J. Heart Fail.* **12**, 789–796 (2010).
34. D'Armiento, J. Matrix metalloproteinase disruption of the extracellular matrix and cardiac dysfunction. *Trends Cardiovasc. Med.* **12**, 97–101 (2002).
35. Harjai, K. J. et al. Does left ventricular shape influence clinical outcome in heart failure? *Clin. Cardiol.* **23**, 813–819 (2000).
36. Koilpillai, C. et al. Relation of ventricular size and function to heart failure status and ventricular dysrhythmia in patients with severe left ventricular dysfunction. *Am. J. Cardiol.* **77**, 606–611 (1996).
37. Groves, A. M. et al. Disruption of intracardiac flow patterns in the newborn infant. *Pediatr. Res.* **71**, 380–385 (2012).
38. Cox, D. J. & Groves, A. M. Inotropes in preterm infants – evidence for and against. *Acta Paediatr.* **101**, 17–23 (2012).
39. Takahashi, Y. et al. Postnatal left ventricular contractility in very low birth weight infants. *Pediatr. Cardiol.* **18**, 112–117 (1997).
40. Bensley, J. G., Stacy, V. K., De Matteo, R., Harding, R. & Black, M. J. Cardiac remodeling as a result of pre-term: implications for future cardiovascular disease. *Eur. Heart J.* **31**, 2058–2066 (2010).
41. Bertagnolli, M. et al. Activation of the cardiac renin-angiotensin system in high oxygen-exposed newborn rats: angiotensin receptor blockade prevents the developmental programming of cardiac dysfunction. *Hypertension* **67**, 774–782 (2016).
42. Miyawaki, M., Okutani, T., Higuchi, R. & Yoshikawa, N. The plasma angiotensin II level increases in very low-birth weight infants with neonatal chronic lung disease. *Early Hum. Dev.* **84**, 375–379 (2008).
43. Hamill, N. et al. Fetal cardiac ventricular volume, cardiac output, and ejection fraction determined with 4-dimensional ultrasound using spatiotemporal image correlation and virtual organ computer-aided analysis. *Am. J. Obstet. Gynecol.* **76**, e1–e10 (2011).
44. Schulz-Menger, J. et al. Standardized image interpretation and post processing in cardiovascular magnetic resonance: Society for Cardiovascular Magnetic Resonance (SCMR) board of trustees task force on standardized post processing. *J. Cardiovasc. Magn. Reson.* **15**, 35.s (2013).